ELSEVIER

Contents lists available at ScienceDirect

# Water Research

journal homepage: www.elsevier.com/locate/watres





# Pilot-scale field demonstration of a hybrid nanofiltration and UV-sulfite treatment train for groundwater contaminated by per- and polyfluoroalkyl substances (PFASs)

Charlie J. Liu <sup>a,d</sup>, Garrett McKay <sup>a,b</sup>, Daqian Jiang <sup>a,c</sup>, Raul Tenorio <sup>a</sup>, J. Tani Cath <sup>a</sup>, Camille Amador <sup>a</sup>, Conner C. Murray <sup>a</sup>, Juliane B. Brown <sup>a</sup>, Harold B. Wright <sup>e</sup>, Charles Schaefer <sup>f</sup>, Christopher P. Higgins <sup>a</sup>, Christopher Bellona <sup>a</sup>, Timothy J. Strathmann <sup>a,\*</sup>

- <sup>a</sup> Department of Civil and Environmental Engineering, Colorado School of Mines, Golden, CO 80401, USA
- <sup>b</sup> Zachry Department of Civil and Environmental Engineering, Texas A&M University, College Station, TX 77843, USA
- <sup>c</sup> Department of Civil, Construction and Environmental Engineering, University of Alabama, Tuscaloosa, AL 35487, USA
- d Kennedy Jenks Consultants, San Francisco, CA 94104, USA
- e Carollo Engineers, Boise, ID 83713, USA
- f CDM Smith, Edison, NJ 08837, USA

#### ARTICLE INFO

# Keywords: PFAS Destruction Membrane Technologies Hydrated Electrons Energy Requirements Emerging Technologies AFFF

#### ABSTRACT

Previous laboratory scale studies indicate nanofiltration (NF) and UV-sulfite photochemical treatments as promising technologies for the removal and destruction, respectively, of per- and polyfluoroalkyl substances (PFASs) from contaminated water. This study reports on a field demonstration of a pilot-scale hybrid NF and UVsulfite treatment train for the remediation of 12 PFASs detected in groundwater impacted by aqueous filmforming foam (AFFF) at a U.S. Department of Defense installation. For most of the detected PFASs, NF rejection was consistently  $\geq$  95% over a 30-day field trial when operating at 90% total permeate recovery. Rejection of short-chain perfluorosulfonic acids (PFSAs) by NF decreased when recoveries increased from 90 to 97%; tests with a reverse osmosis (RO) membrane showed ≥ 99% rejection of all PFASs regardless of increasing recovery. UV treatment of the NF reject following 90% permeate recovery resulted in variable destruction of individual PFASs, with rates also being dependent on pH and the identity and concentration of UV photosensitizer. Rates of perfluorocarboxylic acid (PFCA) degradation were greater than those measured for PFSAs and perfluoroalkyl acid (PFAA) precursors and were independent of perfluoroalkyl chain length. In contrast, rates of PFSA degradation increased with increasing chain length. Consistent levels of PFAS degradation by UV-sulfite were observed during a 30-day demonstration experiment in NF reject water amended with 10 mM sulfite and adjusted to pH 11.2. Collectively, > 75% of the detected PFAS mass in the NF reject was destroyed after 4 h of UV treatment, increasing to > 90% after 8 h of treatment. An analysis of electrical energy inputs for the hybrid NF/UV-sulfite treatment train showed energy per order magnitude (EE/O) requirements ranging from  $\leq 13.1 \text{ kWh/m}^3$  for PFCAs and 14.1 kWh/m<sup>3</sup> for PFOS to values > 100 kWh/m<sup>3</sup> for more recalcitrant short-chain PFSA analogues. The UV reactor and water-cooling system were the major contributors to overall energy requirements and represent the greatest opportunities for improving efficiency of the technology.

#### 1. Introduction

The use of fire-suppressing aqueous film-forming foam (AFFF) at military and domestic fire training areas has contributed to the wide-spread contamination of per- and polyfluoroalkyl substances (PFASs) in water resources worldwide (Barzen-Hanson et al., 2017; Hu et al.,

2016). PFASs are highly recalcitrant and have been associated with various adverse human health effects (USEPA, 2016a, 2016b). As a result, the U.S. Environmental Protection Agency (USEPA) established lifetime health advisory levels (HAL) of 70 ng/L for perfluorooctane sulfonate (PFOS) and perfluorooctanoic acid (PFOA) combined (USEPA, 2016a, 2016b), with individual states setting more stringent guidelines

E-mail address: strthmnn@mines.edu (T.J. Strathmann).

<sup>\*</sup> Corresponding author.

for these and other commonly detected PFASs (Simon et al., 2019).

Conventional water and wastewater treatment methods are largely ineffective at removing PFASs; instead, separation-based advanced water treatment methods such as adsorbents (e.g., granular activated carbon (GAC) and anion exchange resins (AERs)) (Laura Del Moral et al., 2020) and high-pressure membranes (e.g., nanofiltration (NF) and reverse osmosis (RO)) (Liu et al., 2021) are used to treat PFASs. An advantage to high-pressure membranes is the effective rejection of shorter chain PFASs that are less effectively removed by GAC and AER (Laura Del Moral et al., 2020; Liu et al., 2019). Recent work has also shown the effective rejection of a broader suite of PFASs, including many precursors of perfluoroalkyl acids (PFAAs), detected in AFFF using high-resolution mass spectroscopy suspect screening methods (Liu et al., 2021).

There is growing interest in technologies that can degrade PFASs, and active research is underway for development of destructive technologies such as plasma (Nau-Hix et al., 2021), electrochemical (Le et al., 2019), hydrothermal (Wu et al., 2019), and photochemical processes (Tenorio et al., 2020). Recently, the hydrated electron (e<sub>ag</sub><sup>-</sup>), a highly reactive reductant generated by UV photosensitizer processes (E = -2.9 V (Buxton et al., 1988)), has garnered attention due to its ability to reductively defluorinate a wide range of PFASs including perfluorocarboxylic acids (PFCAs), perfluorosulfonic acids (PFSAs), and PFAA precursors (Bentel et al., 2020; Bentel et al., 2019; Cui et al., 2020; Park et al., 2009; Sun et al., 2018; Tenorio et al., 2020). UV photochemical processes can be readily implemented due to the widespread availability of UV lamps and reactors as well as chemical photosensitizers used to generate hydrated electrons (e.g., sodium sulfite). Hydrated electrons may also be generated through the combination of medium pressure UV lamps and an electrode and similarly used to effectively degrade PFASs (Rao et al., 2020; Su et al., 2019). While destruction of PFASs is desirable, direct treatment of contaminated water supplies with these technologies may not be practical due to their large energy requirements per unit volume of water treated (Bentel et al., 2020). Instead, destruction is anticipated to be more practical when applied to treat small volume concentrate streams generated as byproducts of separation-based processes, including membrane reject concentrate streams generated by NF and RO treatment.

To better represent full-scale treatment, pilot-scale assessments of membrane separation and destructive processes are necessary. To date, studies applying high-pressure membranes for PFAS treatment have been largely conducted using bench-scale flat sheet membrane systems (Appleman et al., 2013) that may not be representative of treatment achieved at full-scale using spiral wound membranes due to changing conditions along the length of the element (Fujioka et al., 2014). Similarly, UV-sulfite treatment of PFASs has been primarily limited to small volume (< 1 L) bench-scale reactors treating PFASs spiked into deionized water matrices (Bentel et al., 2020; Sun et al., 2018; Tenorio et al., 2020). Little is known about the degradation of PFASs in real contaminated natural water matrices (e.g., groundwater) using reactors representative of full-scale UV treatment systems.

Based on promising laboratory scale studies demonstrating the effective rejection and destruction of PFASs in AFFF impacted waters by high-pressure membranes (Liu et al., 2021) and UV-sulfite (Tenorio et al., 2020), respectively, this contribution reports the results of a pilot-scale treatment train combining NF and UV-sulfite technologies to treat AFFF-impacted groundwater at a U.S. Department of Defense (DoD) installation. NF was operated in recirculating semi-batch mode to 90% total water recovery, producing a 10% reject byproduct stream that was then fed into a UV reactor amended with sulfite photosensitizer to promote PFAS degradation. Long-term NF and UV operation was monitored and validated over 30 days. The effect of total water recovery on rejection of PFASs by both NF and RO membranes was also assessed. UV treatment of the membrane reject was monitored throughout the study, and the effects of operating conditions including pH and photosensitizer identity and concentration were evaluated. Findings from this

study provide valuable insights into the viability of using these technologies, both separately and combined, for remediation of AFFF-impacted water resources.

#### 2. Methods

#### 2.1. Chemicals

All chemicals were purchased from Sigma-Aldrich (St. Louis, MO). Sodium hydroxide (NaOH, > 97% purity) was used for pH adjustment. Sodium sulfite (Na<sub>2</sub>SO<sub>3</sub>, >9 8%), potassium iodide (KI, > 99.9%), and nitrilotriacetic acid (NTA, > 98%) were used as photosensitizers to generate  $e_{aq}^-$  in separate UV experiments. Most experiments were conducted to treat PFASs present in the source groundwater, but select experiments were performed by spiking groundwater with higher concentrations of five commonly detected PFASs (0.5  $\mu$ g/L), perfluorohexanoic acid (PFHxA, > 98%), perfluorooctanoic acid (PFOA, > 95%), perfluorobutane sulfonate (PFBS, > 97%), perfluorohexane sulfonate (PFHxS, > 98%), and perfluorooctane sulfonate (PFOS, > 98%).

#### 2.2. NF and UV-sulfite treatment train

The NF and UV-sulfite treatment train was deployed at a U.S. DoD installation in Colorado to treat historical AFFF-impacted groundwater at a monitoring well. Fig. 1 shows a simplified process diagram (Auto-CAD®) and photographs of the demonstration system. A supervisory control and data acquisition (SCADA) system (LabVIEW<sup>TM</sup>) was used to automate the treatment train and record process variables. Briefly, a typical 1-day treatment cycle was operated according to the following:

- PFAS-contaminated groundwater was pumped from a monitoring well and stored in a 757 L (200 gal) storage tank.
- 568 L (150 gal) groundwater from the storage tank was pumped through sediment and cation exchange pretreatment cartridge filters into a second 757 L NF concentration tank.
- Water from the NF concentration tank was passed through the NF system in recirculating fashion until 90% permeate recovery was achieved and producing a 10% reject byproduct stream containing concentrated PFASs.
- The resulting NF reject was then transferred to a 57 L (15 gal) UV reactor tank.
- The NF reject was amended with photosensitizer (typically 10 mM sodium sulfite) and NaOH (for pH adjustment) and recirculated through an annular UV reactor for 23 h of treatment prior to discharge. All treated water (NF permeate, UV treated water) was passed through a GAC polishing filter prior to final discharge as a precaution to remove residual PFASs.

#### 2.2.1. Pretreatment

As groundwater is concentrated to high recoveries, fouling/scaling of membranes and UV quartz sleeves due to suspended solids and sparingly soluble salts (primarily  $\text{Ca}^{2+}$  and  $\text{Mg}^{2+}$  precipitates) may adversely impact treatment. To address these concerns, raw groundwater was pretreated by filtering sequentially through 50, 20, and 5  $\mu m$  sediment filters (WB-HB-20 Harmsco) followed by five cation exchange cartridge filters (WS-20BB, Pentek) in series. Multiple cation exchange filters were used to reduce replacement frequency. In full-scale practice, these would likely be replaced by a regenerable ion exchange softening system or other water softening process, but disposable cartridge filters were used here for convenience. Sediment and cation exchange filters were replaced after 30 and 13 days of operation, respectively.

# 2.2.2. NF pilot

The custom-built high-pressure membrane system contained three 2540 (2.5" diameter  $\times$  40" length) spiral wound NF270 membranes (NF;

C.J. Liu et al. Water Research 205 (2021) 117677

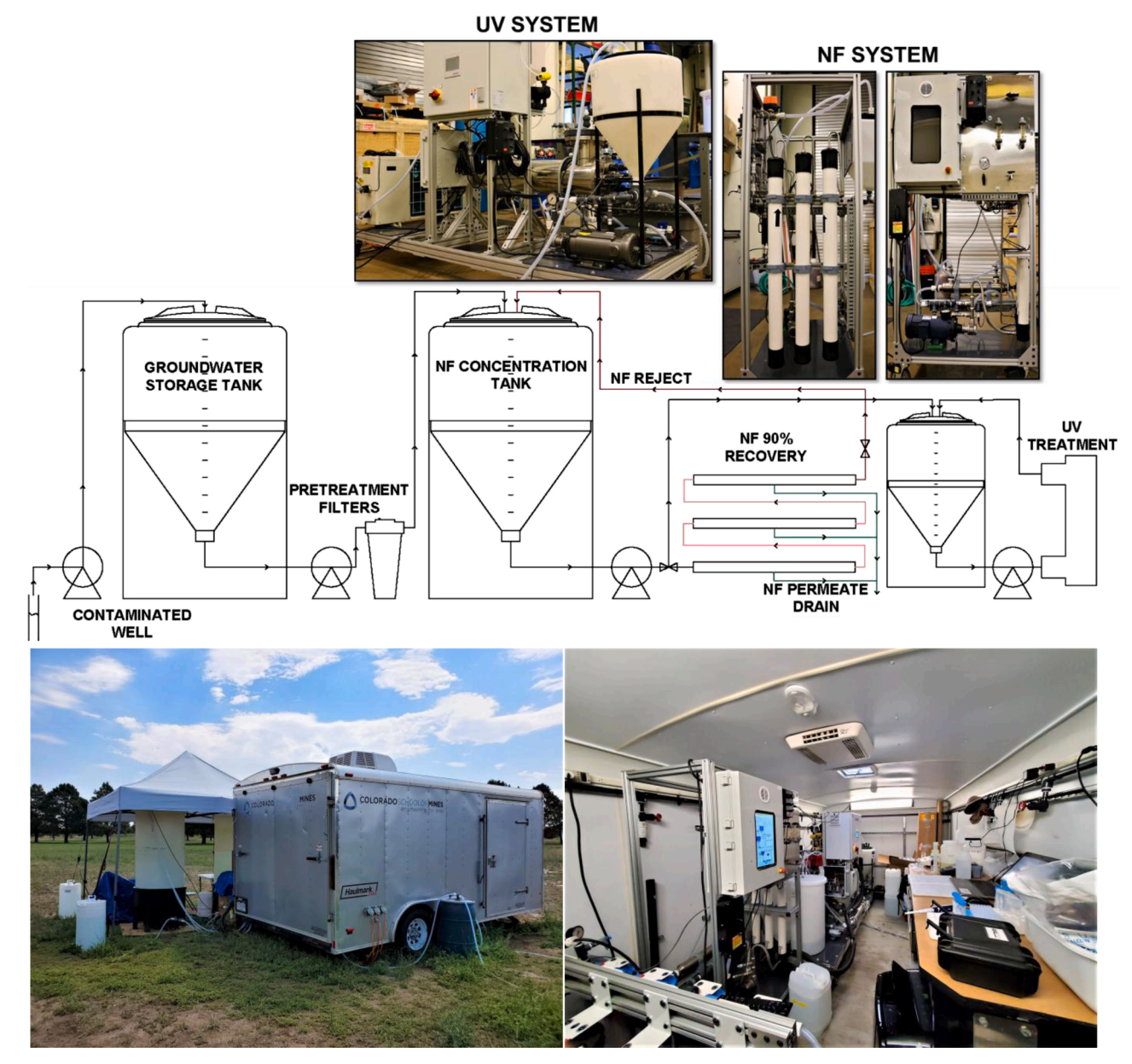


Fig. 1. Simplified process flow diagram and photographs of NF/UV-sulfite pilot system (top), and field deployment photographs (trailer outside, bottom left; trailer inside, bottom right).

DuPont Filmtec, Midland, MI; characteristics provided in the supplementary information (SI) Table S1) and was used to treat 568 L batches of groundwater to 90% total permeate recovery (and yielding 57 L of reject) during each treatment cycle (~3.5 h treatment time). One treatment cycle was conducted per day during the field deployment. All membrane experiments were operated at a conservative single pass permeate flux of 18.8 LMH and 28% single-pass recovery (approximately 6.3 LMH or 9.3% recovery per element with slight differences between membranes in series) and single-pass reject flowrate of 6.2 L/ min. Here, "recovery" or "permeate recovery" refers to the reduction in volume (i.e., generally 90% volume reduction from 568 to 57 L) during NF semi-batch operation whereas "single-pass recovery" is a function of membrane flux and feed flowrate that was fixed at 28% for all experiments. Operating conditions were selected to balance the time required to reach 90% permeate recovery, system operating limitations, and membrane integrity. Separate experiments were conducted to evaluate the effects of increasing recovery up to 97% on rejection of PFASs by both NF and RO (ESPA, Hydranautics, Oceanside, CA; Table S1)

membranes using the aforementioned operating conditions but at slightly longer operating times to achieve the higher recovery.

# 2.2.3. UV pilot

A pilot-scale UV system (LBX 90e) consisting of a UV reactor, electrical control box, and wiper was obtained from Xylem Inc. (Rye Brook, NY) and mounted on a custom-built skid. The reactor contained four, 330 W low-pressure high-output mercury lamps (ELR-30) generating  $\lambda=254$  nm wavelength light (no ozone generation) installed in quartz sleeves that were cleaned hourly with a mechanical wiping mechanism. The reactor was equipped with a UV intensity sensor  $(W/m^2)$  placed in the middle of the reactor and the lamps were operated at 100% power for all experiments. All UV treatment experiments were performed using 57 L of reject following 90% recovery from the NF system, which was transferred into a 57 L tank where NaOH (pH adjustment) and the selected chemical sensitizer, usually sodium sulfite, were dosed. The dead volume of the reactor was approximately 45 L. Including chemical additions, the total UV treatment volume for each cycle was  $\sim 59$  L. No

gas sparging of the UV reactor or reject to remove dissolved oxygen was performed before UV treatment. The UV water temperature was maintained at  $26.5\pm0.5^{\circ}\text{C}$ . Water was recirculated through the UV reactor for 23 h at 14.4 Lpm (3.8 gpm). Initial experiments were performed to assess the impact of pH, sulfite concentration, and chemical sensitizer identity on treatment and to identify optimal treatment conditions. Long-term 30-day experiments were then performed at the optimal conditions identified. Table S3 summarizes estimated UV doses and dose-based rate constants and Table S6 lists measured UV intensity, UV254 %T, and sulfite concentration.

#### 2.6. Water analysis

Targeted PFAS analysis (50 compounds) and suspect screening (protocols described elsewhere (Liu et al., 2021)) were performed by liquid chromatography quadrupole time-of-flight mass spectrometry using authentic reference standards (LC-QToF-MS; SCIEX (Framingham, MA) X500R QTOF system). Additional information on PFAS analytical methods, limits of quantification (LOQ) (Table S2), and general water quality parameter measurements can be found in the SI.

#### 3. Results and discussion

#### 3.1. Groundwater characterization

Twelve PFASs were quantified in the source groundwater including 4 PFCAs (PFPeA, PFHxA, PFHpA, and PFOA), 6 PFSAs (PFPrS, PFBS, PFPeS, PFHxS, PFHpS, and PFOS), and 2 PFAA precursors (FHxSA and 6:2 FTS). Suspect screening analysis of the groundwater was also conducted, but no additional compounds could be confidently identified. PFAS concentrations in the groundwater source were monitored for 30 days and did not vary significantly as shown in Fig. S1A and B; average concentrations are listed in Table 1. Concentrations of PFSAs were generally higher than PFCAs, as reported in many historical AFFF-usage sites (Hu et al., 2016). The presence of odd and even chain PFASs, elevated concentrations of even chain PFSAs (i.e., PFHxS, PFOS), and the presence of a fluorotelomer sulfonate detected in the groundwater indicates site contamination from AFFFs produced by both electrochemical fluorination and telomerization processes (Moody and Field, 2000). Analysis of general water quality parameters showed no

**Table 1**PFAS concentrations in groundwater and NF reject<sup>a</sup>.

PFAS	Acronym	MW (g/ mol)	Groundwater (ng/L)	NF Reject (ng/L)
Perfluoropentanoic acid	PFPeA	264	$11.9 \pm 2.4$	$71.8 \pm \\10.7$
Perfluorohexanoic acid	PFHxA	314	$12.0\pm3.1$	$71.5 \pm \\12.5$
Perfluoroheptanoic acid	PFHpA	364	$6.0\pm1.8$	$38.2 \pm 5.7$
Perfluorooctanoic acid	PFOA	414	$3.6\pm0.9$	$23.0\pm4.1$
Perfluoropropane sulfonate	PFPrS	250	$1.5\pm0.9$	$8.9 \pm 2.4$
Perfluorobutane sulfonate	PFBS	300	$8.3 \pm 2.4$	$52.7 \pm 10.5$
Perfluoropentane sulfonate	PFPeS	350	$3.6\pm1.0$	$22.4 \pm 4.6$
Perfluorohexane sulfonate	PFHxS	400	$23.9 \pm 4.1$	$173.0 \pm \\36.3$
Perfluoroheptane sulfonate	PFHpS	450	$1.0\pm0.2$	$6.1\pm1.2$
Perfluorooctane sulfonate	PFOS	500	$25.5 \pm 3.4$	$189.4 \pm \\43.1$
Perfluorohexane sulfonamide	FHxSA	399	$26.1\pm3.6$	$156.8 \pm \\31.1$
6:2 Fluorotelomer sulfonate	6:2 FTS	428	$1.2\pm1.3$	$16.1 \pm 4.0$

 $<sup>^{\</sup>rm a}$  Average values with standard deviations from n=13 samples collected over 30 days.

significant variations over the course of the field trial (Table S4). PFAS concentrations did not change following pretreatment by sediment and cation exchange filters (data not shown); the major effect of pretreatment was the desired removal of Ca<sup>2+</sup> and Mg<sup>2+</sup> by the cation exchange cartridges. It is also worth noting that PFAS concentrations in the source water at the time of the field trial were appreciably lower than those measured during site selection activities conducted prior to deployment, indicating transiency of the PFAS source at the site. Regardless, the sensitivity of the LC-QToF-MS methods allowed for analysis of treatment efficacy despite the low initial PFAS concentrations.

#### 3.2. High-pressure membrane performance

#### 3.2.1. Impact of recovery on rejection of PFASs

Initial experiments were performed to evaluate the impact of total system permeate recovery on the rejection of PFASs by NF and RO. Rejection as a function of recovery from 90 to 97% is shown in Fig. 2 for NF (2A and B) and RO (2C and D). Both membranes were operated at the same conditions (18.8 LMH permeate flux and 6.2 L/min reject flowrate) and rejection was calculated using the LOQ concentration when measured PFAS concentrations were < LOQ (Table S2). Rejection of PFASs by NF, calculated using the influent and permeate concentrations at the specified recovery, was > 95% at all recoveries, with the exception of shorter chain PFSAs (PFBS and PFPrS) which were rejected between 88 and 93%. As recovery was increased to 97%, rejection of shorter chain PFASs (PFPrS, PFBS, PFPeA, PFHxA) by NF decreased (Fig. 2A and B), likely due to the increased concentration of PFASs and dissolved ionic species in the concentrated feed stream (Liu et al., 2021). However, rejection of longer chain PFASs was not significantly affected when operating at higher recoveries, possibly due to an enhanced sieving effect from foulants such as dissolved organic carbon (DOC) (Appleman et al., 2013).

Previous work demonstrated the effective rejection of PFASs by RO to permeate concentrations <LOQ (Liu et al., 2021). Thus, to enhance the likelihood of detecting PFASs in RO permeate, five PFASs (PFHxA, PFOA, PFBS, PFHxS, and PFOS) were spiked into the groundwater at concentrations of 0.5  $\mu$ g/L each prior to evaluating RO performance. Even with the elevated feed concentrations, observed rejection of all PFASs by RO was > 99% regardless of permeate recovery, demonstrating superior rejection of RO compared to NF (Fig. 2C and D).

A combination of electrostatic repulsion and size exclusion likely contributes to the overall high rejection of PFASs by NF and RO membranes (Appleman et al., 2013). Electrostatic repulsion occurs between the negatively charged membrane polymers at groundwater pH 7.3 (Table S1) and the anionic PFCAs, PFSAs, and 6:2 FTS. Because FHxSA is likely neutral at pH 7.3 (Nguyen et al., 2020) due to the sulfonamide headgroup, rejection by NF was consistently lower than the anionic analogue, PFHxS, attributed to the lack of an electrostatic repulsion rejection mechanism for this compound (Fig. 2B). The effective rejection of PFASs due to size exclusion by NF and RO is consistent with the molecular weights of PFASs evaluated in this study (250–500 g/mol) being higher than the molecular weight cutoff of the NF (180 g/mol) and RO (100 g/mol) membranes (Table S1). Increased size exclusion is likely responsible for the higher rejection observed for longer chain PFASs by NF.

Although RO was more effective than NF in rejecting PFASs, RO requires higher operating pressures than NF (Liu et al., 2021) and retains greater concentrations of groundwater constituents measured at 97% permeate recovery such as sodium (3000 mg/L compared to 1700 mg/L), nitrate (370 mg/L compared to 4 mg/L), silica (270 mg/L compared to 12 mg/L), and DOC (>100 mg/L compared to 37 mg/L) (Table S5) in the RO concentrate than in the NF concentrate. High concentrations of these groundwater constituents can promote more membrane fouling/scaling, introduce greater concentrate management challenges, and inhibit photochemical treatment of PFASs in the reject stream. For example, preventing accumulation of nitrate in the

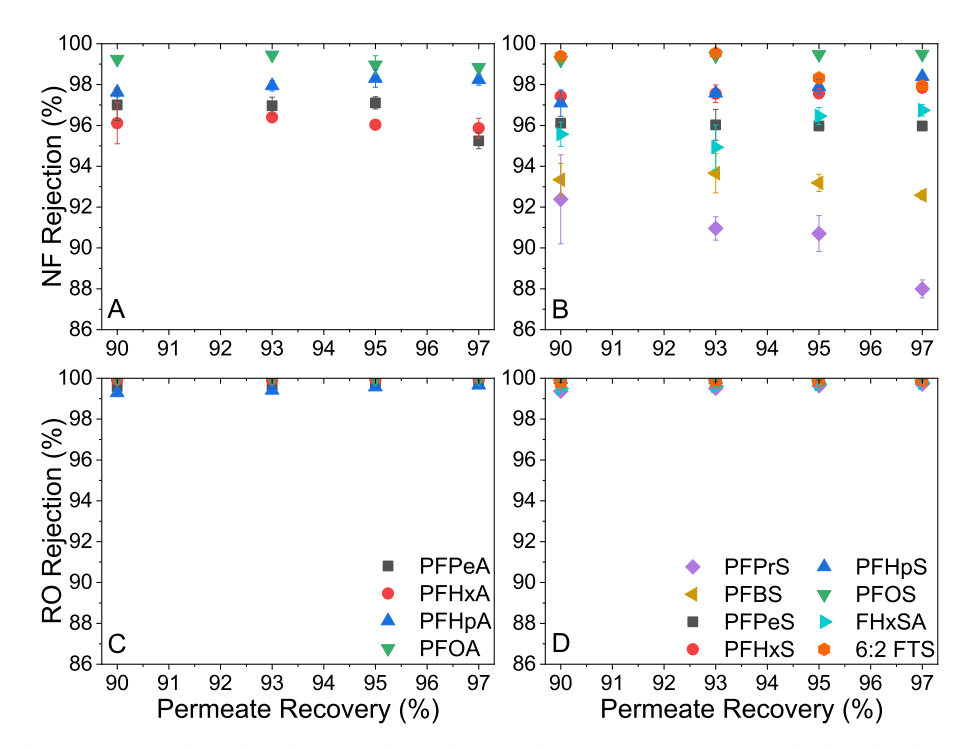


Fig. 2. Rejection of PFASs by NF (upper panels) and RO (lower panels) as a function of permeate recovery. Left panels show data for PFCAs and right panels show data for PFSAs and PFAA precursors. Membrane operating conditions: 18.8 LMH single pass flux and 6.2 L/min single pass reject flowrate. Uncertainties represent min/max values observed in duplicate experiments.

membrane reject (much lower concentration in NF reject than RO reject) is critical because nitrate is an effective scavenger of  $e_{aq}-$  (Cui et al., 2020).

#### 3.2.2. NF long-term performance

Following the tests described above, the NF pilot system was operated to 90% permeate recovery to achieve PFAS removal, while minimizing potential for membrane fouling. To evaluate long-term performance of the NF/UV-sulfite treatment train, one treatment cycle was performed in an automated fashion each day for 30 consecutive days. One treatment cycle consists of concentrating groundwater to 90% permeate recovery by the NF membrane followed by UV-sulfite treatment of the NF reject. On 13 of the 30 days, samples were collected for analysis to assess performance of the NF and UV-sulfite unit processes; 30-day treatment performance of UV-sulfite is discussed later in Section 3.3.4. Fig. 3 depicts rejection of PFASs by the NF membrane over 30 days showing both permeate concentrations (open symbols) and rejection % (closed symbols). Corresponding PFAS concentrations in the NF reject stream are shown in Fig. S1C and D and average concentrations are listed in Table 1. Rejection of individual PFASs was generally consistent over the 30 concentration cycles. Average rejection varied between 92 and 98% for individual PFASs, consistent with those shown in Fig. 2. Longer chain PFASs were rejected to a higher degree than shorter chain analogues. Comparison of the NF reject concentrations and the raw groundwater (Table 1) shows that PFASs were concentrated in the byproduct reject stream, increasing by a factor consistent with 90% recovery and the measured permeate concentrations (Fig. 3). Concentrating PFASs to a small volume reject stream is expected to reduce the requirements for UV treatment PFAS mass reduction goals.

A temporary decrease in rejection of PFASs was observed around day 6, corresponding to operational error when cation exchange cartridge filter change-out was delayed resulting in breakthrough of  $\mbox{Ca}^{2+}$  and  $\mbox{Mg}^{2+}$  in the NF feed stream (Table S4). Divalent cationic species such as  $\mbox{Ca}^{2+}$  and  $\mbox{Mg}^{2+}$  have been shown to decrease rejection of organic compounds due to reducing negative membrane surface charge or by forming DOM-Ca $^{+2}$  complexes causing increased membrane fouling

(Lee et al., 2005). Rejection values observed in the field (92–98%) were similar to those reported recently for treatment of a similar groundwater performed in the laboratory (Liu et al., 2021).

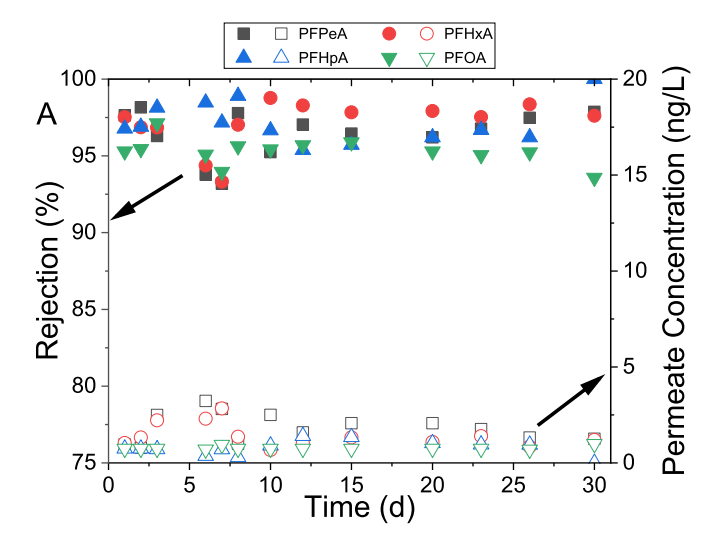
A small initial increase in membrane permeability, as represented by temperature corrected specific flux (Eq. (S1)), was observed in the first 5 concentration cycles followed by small, but continuous decrease in the subsequent 25 concentration cycles (Fig. 4). The small decline in membrane permeability suggests membrane fouling occurred, and that longer term operation might benefit from modifying operating conditions such as reducing single-pass membrane recovery (~9.3% per element), reducing total system permeate recovery (90%), increasing crossflow velocity (6.2 L/min reject flowrate), or changing membrane cleaning protocols which consisted only of daily membrane system flushes for 15 min. Still, results show that the NF system can reliably recover 90% permeate while effectively rejecting PFASs over an extended period of operation.

# 3.3. UV treatment of PFASs in NF reject

#### 3.3.1. General trends and impact of pH on UV-sulfite treatment

Tests were first conducted to optimize UV treatment of PFASs that accumulated in the NF reject stream (byproduct following 90% permeate recovery). A pseudo-first-order kinetic model was applied to obtain rate constants for individual PFASs in all treatment conditions. Fig. 5 shows the effects of pH (Fig. 5A and B), photosensitizer identify (Fig. 5C and D), and sulfite dose (Fig. 5E and F) on the observed rate constants for degradation of individual PFASs ( $k_{\rm obs}$ ,  $h^{-1}$ ); a complete listing of rate constants is provided in Table S8, and measured residual concentrations at each sampling time are shown in Figs. S2–4.

Degradation of PFCAs occurred more quickly than PFSAs and PFAA precursors under all conditions, with no apparent difference being noted for PFCAs of different chain lengths (Fig. 5A). In contrast, rates of degradation observed for PFSAs increased with increasing chain length (Fig. 5B). Observed degradation trends among the different PFASs are consistent with earlier reports using laboratory batch reactors and deionized matrix solutions (pH 9.5) amended with various PFASs and



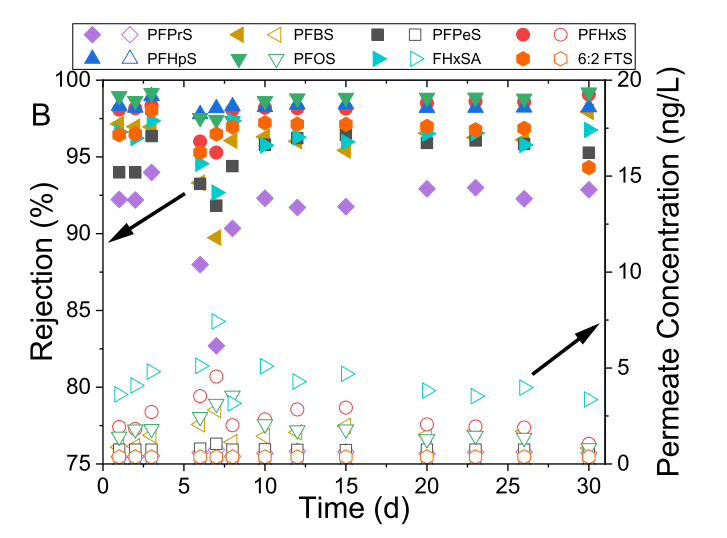


**Fig. 3.** Rejection and permeate concentrations of PFASs measured for 90% permeate recovery over 30 days of treatment for (A) PFCAs and (B) PFSAs and PFAA precursors. Membrane operating conditions: 18.8 LMH single pass flux and 6.2 L/min single pass reject flowrate. Permeate concentrations set at LOQ values (Table S2) for individual PFASs when not detected.

AFFF mixtures (Bentel et al., 2019; Tenorio et al., 2020). FHxSA, a sulfonamide-based PFAS, degraded at a similar rate as PFHxS (Fig. 5B), indicating that the sulfonamide head group (both have a 6-C perfluorinated chain) does not have significant impact on degradation. However, the degradation rate constants measured for 6:2 FTS, which also has a 6-carbon polyfluorinated chain, were less than those measured for FHxSA and PFHxS possibly due to the generation of 6:2 FTS (C/C<sub>0</sub>> 1 at early timepoints, Fig. S2D) during UV treatment. Transient generation of 6:2 FTS and other PFASs during UV-based treatment processes in AFFF-impacted waters has been observed in laboratory studies (Tenorio et al., 2020), and attributed to the conversion of 6:2 FTS precursors that were not identified using the existing LC-QToF-MS targeted or suspect screening analysis methods. The slower degradation of 6:2 FTS compared to PFHxS may also be attributed to the presence of a non-fluorinated -CH2CH2- group adjacent to the sulfonate headgroup, similar to findings in a recent report showing slower degradation of fluorotelomer carboxylic acids (FTCAs) compared to fully fluorinated PFCAs (Bentel et al., 2019).

The pH of the NF reject prior to UV-sulfite treatment had a pronounced effect on degradation of PFASs, with  $k_{\rm obs}$  values for PFCAs increasing  $\sim$ 6-fold when pH was increased from 9.5 to 11.2 prior to UV

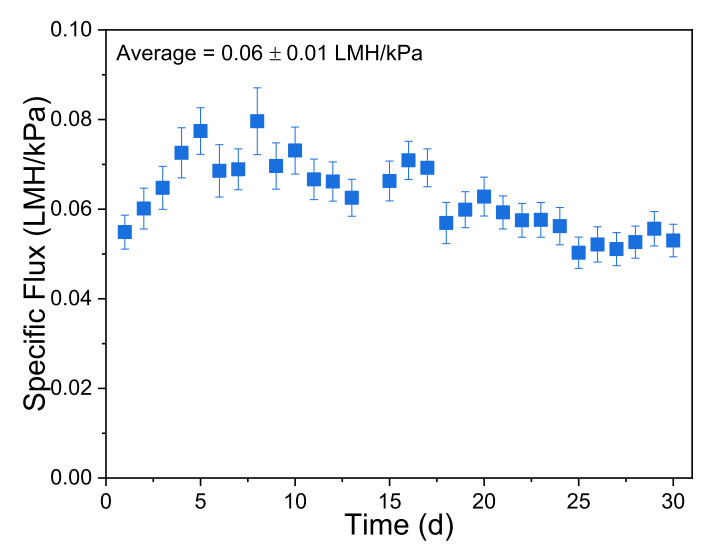


Fig. 4. Membrane specific flux (temperature corrected) measured over 30 days. Each data point represents the average specific flux measured over the operating time ( $\sim$ 3.5 h). Uncertainties represented as standard deviations. Membrane operating conditions: 18.8 LMH single pass flux and 6.2 L/min single pass reject flowrate.

treatment. The effect for PFOS was even more dramatic, increasing ~12-fold from pH 9.5 to 11.2. Previous laboratory-scale studies have also observed similar enhancement in reaction rates in alkaline conditions (Bentel et al., 2020; Qu et al., 2014). Although the underlying mechanism is still under investigation, Bentel et al. (2020) attributed the increase in reaction rate of PFCAs (PFSAs were not investigated) in alkaline conditions (pH 12) to an increase in the probability of a decarboxylation-hydroxylation-elimination-hydrolysis degradation pathway occurring, thereby cleaving more C-F bonds in the PFAS.

#### 3.3.2. Impact of chemical sensitizer

Alternative photosensitizers for  $e_{aq}^{\phantom{\dagger}}$  generation, including nitrilotriacetate (NTA) (Sun et al., 2018) and potassium iodide (KI) (Qu et al., 2010), were compared with sulfite (Fig. 5C and D) at equimolar concentrations (i.e., 10 mM). Compared to UV-sulfite, degradation of PFCAs in UV-NTA was ~1.5 times faster, whereas PFSAs and PFAA precursors were degraded more slowly using NTA than sulfite. This finding contrasts with earlier laboratory studies showing faster degradation of PFOS in deionized water matrix amended with NTA compared to sulfite (pH 10, 2 mM photosensitizer) (Sun et al., 2018). The inconsistencies in treatment may be attributed to interactions between NTA and groundwater matrix constituents or differences in operating conditions (pH 10 and 2 mM NTA (Sun et al., 2018) compared to pH 11.2 and 10 mM NTA (this study)). However, it is worth noting that UV photolysis of NTA produces pungent odors, likely as a result of amine or urea byproducts, and may pose practical challenges for treatment applications. In comparison, the major byproduct of sulfite photolysis is sulfate, which is ubiquitous in most groundwaters. In contrast to sulfite and NTA, little to no degradation of any of the PFASs was observed when KI was used as the photosensitizer, in contrast to prior laboratory studies (Qu et al., 2014, 2010). The lack of reactivity may be due to enhanced scavenging of e<sub>aq</sub> by iodide intermediates when applying KI concentrations higher than 0.3 mM (Qu et al., 2010). Collectively, results support the use of sulfite as the optimal UV sensitizer for PFAS treatment in this groundwater.

# 3.3.3. Impact of sulfite concentration

Finally, tests evaluated the effects of varying sulfite dose at pH 11.2. A UV-only control (no sulfite added) showed only a small amount of degradation for PFCAs after  $\sim$ 8 h of irradiation time (Fig. S5), consistent

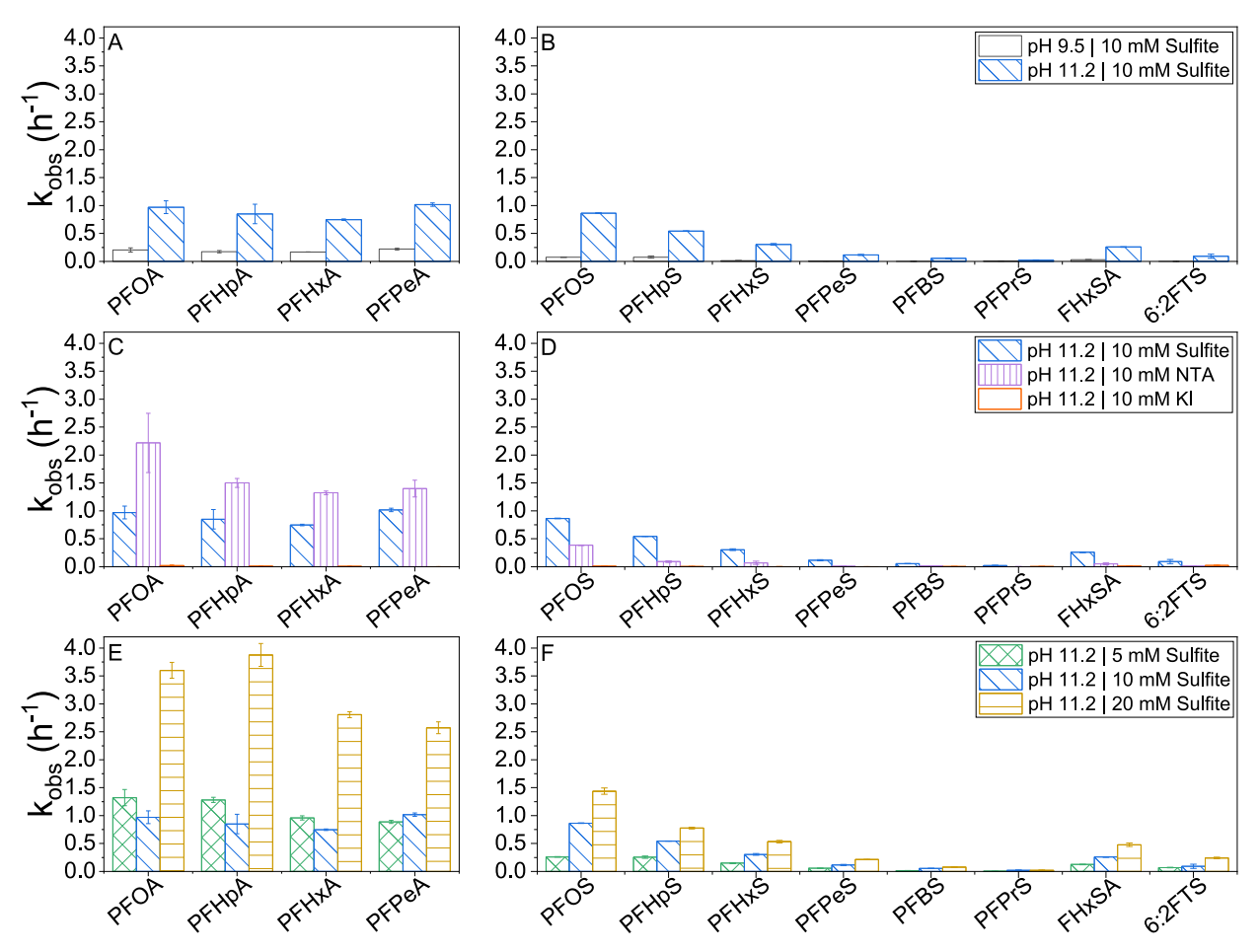


Fig. 5. Impact of pH (panels A,B), photosensitizer identity (panels C,D), and sulfite concentration (panels E,F) on the observed rate constants for degradation of PFCAs (left panels) and PFSAs and PFAA precursors (right panels). Uncertainties represent min/max values measured in duplicate experiments at each condition. Due to rapid degradation, PFCA rate constants were estimated using only 2 samples (t = 0 and 1 h) for experiments with sulfite at pH 11.2 (measured concentrations < LOQ at  $t \ge 2$  h).

with earlier reports (Bao et al., 2018; Guo et al., 2019; Qu et al., 2014, 2010). This also shows that  $e_{aq}^-$  generated from photolysis of organic matter (Zepp et al., 1987) did not contribute significantly to PFAS degradation. Increasing sulfite concentration from 5 to 20 mM generally resulted in increased degradation rates (Fig. 5E and F). For PFCAs, degradation rates were similar at 5 and 10 mM sulfite but increased 3-fold when the sulfite concentration increased to 20 mM. For PFSAs and PFAA precursors, degradation rates doubled between 5 mM and 10 mM sulfite, but then increased less dramatically ( $\sim$ 1.5x) when sulfite was increased to 20 mM. These enhancements in PFAS transformation rate are likely the result of an increased rate of  $e_{aq}^{\phantom{\dagger}}$  formation due to higher sulfite concentrations. However, at higher sulfite concentrations, light absorption begins to plateau resulting in diminishing returns (UV<sub>254</sub> %T  $=69.8\pm0.5\%$  (5 mM),  $50.8\pm3.7\%$  (10 mM),  $34.2\pm0.3\%$  (20 mM)). In contrast, previous bench-scale studies have reported either no significant increases in PFAS treatment at sulfite concentrations > 10 mM (Tenorio et al., 2020) or only slight improvements (i.e., ~10%) (Gu et al., 2017). The discrepancies may be attributed to the multiple high wattage lamps (4  $\times$  330 W) used in this study that provide more photons to react with the higher sulfite concentrations and generate more  $e_{aq}^{-}$ for PFAS degradation compared to the single low wattage lamps (10-18 W) used in the bench-scale studies. Given the fast degradation of PFCAs compared to PFSAs, system operating conditions will generally be dictated by PFSA removal where increased sulfite concentrations > 10 mM has limited benefit. Thus, longer-term tests were conducted using NF reject adjusted to pH 11.2 and amended with 10 mM sulfite before UV irradiation.

## 3.3.4. UV-sulfite long-term performance

Automated UV-sulfite treatment of the NF reject generated daily for 30 consecutive days was performed to assess stability of the treatment system. Degradation trends of PFASs by UV-sulfite were consistent over 30 days as shown in Fig. 6 for select PFASs and reflected treatment trends observed in validation experiments already discussed (Fig. 5). PFCAs were consistently removed within 2 h of treatment regardless of compound chain length, and PFSAs were degraded according to chain length, with PFOS being removed within 4 h (averaged C/C<sub>0</sub> values for all PFASs shown in Fig. S6, concentrations listed in Table S7). Although shorter chain PFSAs were more calcitrant, mass reductions of shorter chain PFSAs were still significant with ~75% of PFHxS and ~20% of PFBS degraded after 4 h of treatment. After 23 h, only PFPrS and PFBS remain in solution with  $\sim$ 50% and  $\sim$ 70%, respectively, degraded in 23 h (Fig. S6). The majority (55%) of total quantified PFAS mass was removed in the first 2 h of treatment, increasing to 76% in 4 h, 90% in 8 h, and 97% after 23 h (Fig. 7). The consistent treatment of PFASs by UVsulfite over 30 days indicates minimal accumulation of foulants on the quartz sleeves and that pretreatment efforts (sediment and cation exchange cartridge filters) and automated sleeve wiping (hourly) were effective at sustaining overall system performance.

Concentrations of the sulfite sensitizer were also monitored during UV-sulfite treatment. A consistent  $\sim 2.5$  mM sulfite loss at the beginning of each reaction was observed (Table S6), possibly attributed to sulfite reaction with dissolved oxygen present in the NF reject water (no effort was made to deoxygenate with gas sparging, a common practice in laboratory experiments). A separate experiment performed by spiking

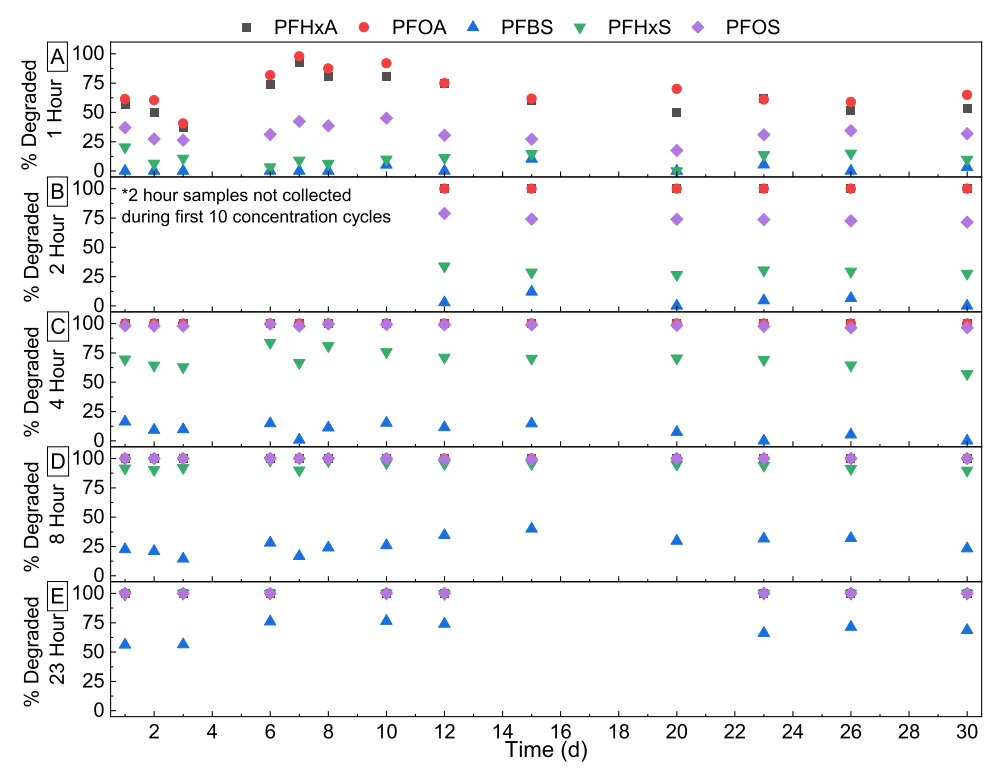


**Fig. 6.** Consistency of UV-sulfite treatment data throughout the 30-day demonstration study. Individual panels show the extent of degradation observed for selected PFAAs after different UV-sulfite treatment times throughout the 30-day demonstration study: (A) after 1 h, (B) after 2 h, (C) after 4 h, (D) after 8 h, and (E) after 23 h. Note that samples after 2 h of treatment were not collected for the first 10 days of the field study (n = 6), and samples after 23 h of treatment were only collected on select days (n = 8). UV operating conditions: 10 mM sulfite, pH 11.2.

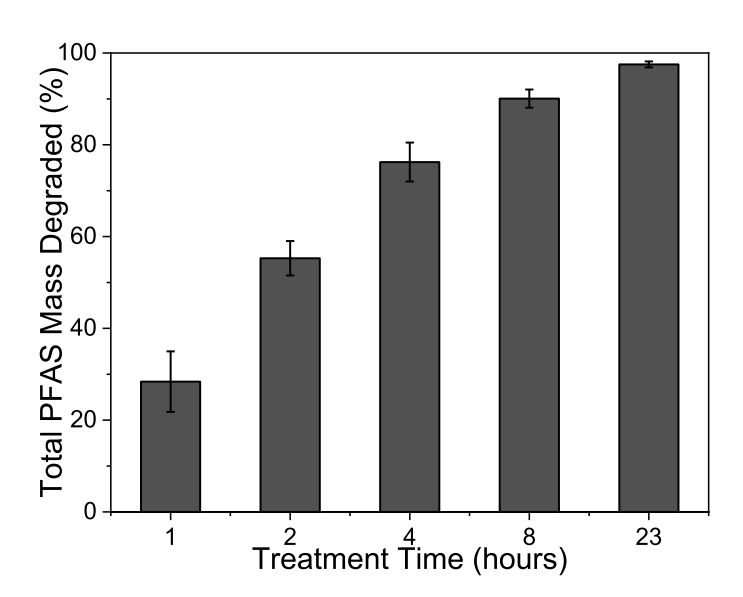


**Fig. 7.** Total extent of PFAS mass reduction (% of PFAS mass initially measured in the NF reject) observed after UV-sulfite treatment for different lengths of time. Uncertainties represent the standard deviation from the average of 13 treatment cycles measured over the 30-day field study. UV operating conditions: 10 mM sulfite, pH 11.2.

sulfite into an aliquot of deoxygenated (N<sub>2</sub> sparged) reject water confirmed no oxidation of sulfite by other water matrix constituents. Although water could be actively deoxygenated by inert gas sparging, results suggest that sulfite addition is an efficient strategy for removing dissolved oxygen. Upon UV irradiation, sulfite concentrations decayed slowly, following a pseudo-first-order rate law ( $k_{obs}=0.075\pm0.027$  h<sup>-1</sup>, R<sup>2</sup> = 0.97  $\pm$  0.02) and decreasing to 1.6  $\pm$  0.7 mM after 23 h of irradiation. Further work is suggested to optimize dosing schemes to accelerate PFAS degradation and/or minimize unreacted residuals in the treated water.

#### 3.4. Electrical costs and treatment outlook

Results from the 30-day continuous treatment experiments were used to determine energy requirements for the overall hybrid NF/UV-sulfite treatment process, where NF was operated to 90% permeate recovery and the times required to destroy 90% of individual PFASs during UV-sulfite treatment of the reject water were used to estimate electrical energy per order (EE/O) (kWh/m³) values for treatment of individual

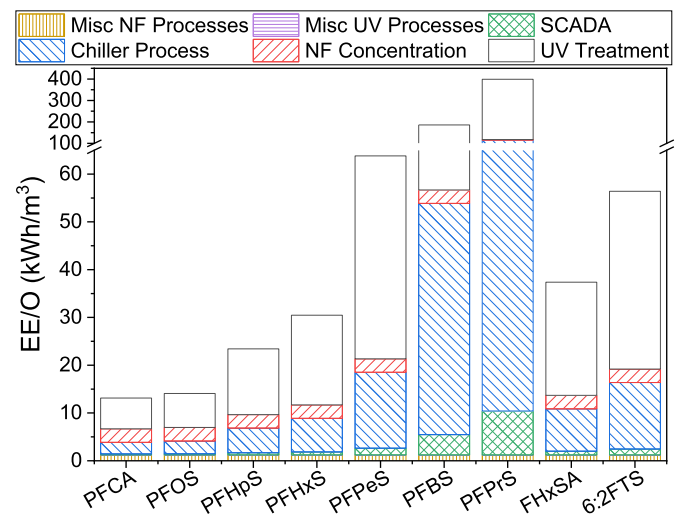


**Fig. 8.** Aggregate and process-specific EE/O (kWh/m³) values for NF/UV-sulfite treatment of PFASs in groundwater. Volume used for EE/O calculation was 568 L. Contribution of NF is consistent for all PFASs, whereas UV and UV-dependent components vary based upon the time required for 90% reduction in concentration of the specific PFAS during UV-sulfite treatment (pH 11.2 and 10 mM sulfite). UV treatment times based on the average rate constants observed throughout the 30-day field study listed in Table S8. Due to the 2-point  $k_{\rm obs}$  derivation for PFCAs, EE/O values for PFCAs assume a UV-sulfite treatment time of 2 h.

C.J. Liu et al. Water Research 205 (2021) 117677

PFASs. The volume used to calculate EE/O was the total volume of water treated, 568 L (150 gal). Fig. 8 shows the results of EE/O estimates for each of the target PFASs, considering all electrical draws required for the treatment train including miscellaneous NF- and UV-associated operations, water chilling, and SCADA control (detailed energy consumption breakdowns in Table S9). Differences in EE/O estimates between individual target PFASs reflect the varying UV-sulfite reaction times required to achieve 90% reduction in concentration (based on 30 day  $k_{obs}$  values, Table S8). A single EE/O value is estimated for PFCAs evaluated in this study (C5–C8) using a treatment time of 2 h due to rapid degradation of these compounds (Fig. 6).

In aggregate, required EE/O values were similar for PFCAs (13.1 kWh/m³) and PFOS (14.1 kWh/m³). Energy requirements for treatment then increased with decreasing chain length for PFSAs, with EE/O values roughly doubling for every decrease in -CF2- in PFSA carbon chain length, reflecting the inertness of these structures to UV-sulfite treatment. Thus, while UV-sulfite treatment of NF reject concentrates may be viable for PFCAs and longer-chain PFSAs (e.g., PFHxS and longer), treatment of the shorter-chain PFSAs such as PFPrS and PFBS would likely be prohibitively energy intensive (EE/O >100 kWh/m³). EE/O values for FHxSA and 6:2 FTS were much greater than that estimated for PFHxS, respectively, again reflecting the differences in  $k_{\rm obs}$  values measured for these PFASs indicating a pre-oxidation step may be considered for more cost-effective removal of these compounds.

Examining the different contributing factors to the total energy requirements, the energy requirements for the NF membrane process was 2.8 kWh/m³ to achieve 90% permeate recovery, or  $\sim$ 20% of the total energy requirements for PFCA and PFOS EE/O. NF energy requirements would vary with recovery due to variable treatment times. In comparison, the UV reactor and associated water-cooling needs represent the major contributors to the energy requirements for treatment. While water cooling, mainly of the UV reactor, was a significant source of energy consumption ( $\sim$ 37%), it is possible that most of these inputs could be eliminated in an optimized full-scale process where passive cooling could be used as an alternative (e.g., using the much larger NF permeate flow as a coolant stream). UV LED technologies may also be used to reduce the energy costs associated with treatment as the technology advances and becomes more cost effective than traditional mercury lamps.

Results from a recent laboratory-scale UV-sulfite study (treating 600 mL of water with 18 W LP UV lamp; pH 12 and 10 mM sulfite) reported an EE/O for PFOA of 15.8 kWh/m $^3$  (Bentel et al., 2020), which is  $\sim$ 2.5 times greater than the 6.44 kWh/m<sup>3</sup> observed here for the UV-sulfite process alone (Table S9). This suggests that there are efficiencies gained by combining NF and UV-sulfite for treatment or by pilot-scale reactor configuration. Results also show that the hybrid NF/UV-sulfite treatment train compares favorably with EE/O values reported recently for other destructive technologies (not operated as a treatment train), including a pilot-scale demonstration of a plasma technology for treatment of PFOA and PFOS ( $16 \pm 6 \text{ kWh/m}^3$ ) (Nau-Hix et al., 2021), pilot-scale photocatalytic process for treatment of PFOA (51  $\pm$  5 kWh/m<sup>3</sup>) (Qanbarzadeh et al., 2020), and bench-scale electrochemical oxidation of PFOA and PFOS (5.1 and 6.7 kWh/m<sup>3</sup>, respectively) (Le et al., 2019). As discussed previously, EE/O calculations for this study were based on the total volume of water treated (568 L) rather than the concentrated volume of water treated in the UV reactor (57 L) indicating that energy costs for PFAS degradation are less by the combination of NF and UV-sulfite than by UV-sulfite itself. If EE/O values were instead calculated based on volume of water treated by UV only, then EE/O values for UV treatment would be 10 × greater (i.e., 64.4 kWh/m<sup>3</sup> for PFOA and 71.2 kWh/m<sup>3</sup> for PFOS).

Destruction of PFASs remains highly energy intensive when compared with other water treatment operations; for context, RO seawater desalination requires 2.5–4 kWh/m $^3$  (Zarzo and Prats, 2018). From an operating perspective, the high UV doses required for treatment (accumulated  $\sim$ 128,000 mJ/cm $^2$  over 2 h and 282,000 mJ/cm $^2$  over 4 h

for PFCA and PFOS degradation, respectively, Table S3) indicate significant challenges to utilizing UV-sulfite in existing single-pass UV disinfection facilities or as a replacement for existing PFAS remediation strategies such as continuous-flow adsorption-based treatment technologies. Additionally, pH adjustment to 11.2 and subsequent neutralization may incur additional operating challenges and costs. Nevertheless, this study demonstrates that both NF and UV-sulfite may be more viable PFAS treatment technologies when combined. High-pressure membranes are not frequently used for PFAS treatment due to concentrate management challenges. UV-sulfite treatment, and by extension other destructive technologies, may leverage the benefits of waste volume reduction to reduce energy requirements for PFAS mass destruction operations.

#### 4. Conclusion

This contribution reported on the results of a field demonstration pilot-scale hybrid NF/UV-sulfite treatment train for the separation and destruction of PFASs from AFFF-impacted groundwater. Initial tests showed that high-pressure membranes can achieve good rejection (> 95%) of most PFASs at high permeate recoveries, with performance being sustained throughout a 30-day consecutive field trial. PFASs were concentrated in the resulting NF reject stream, significantly reducing the volume of water requiring further treatment. PFAS destruction was accomplished by UV treatment after amending the NF reject with sulfite photosensitizer (to generate  $e_{aq}^{\,-})$  and adjusting to alkaline pH conditions (pH 11.2). Rates of destruction observed for individual PFASs were consistent with trends reported in small-scale laboratory studies, with PFCAs and longer-chain PFSAs being readily degraded, while shorterchain PFSAs and 6:2 FTS were degraded much more slowly. Sulfite proved to be a preferable sensitizer to NTA and KI, and treatment at lower pH conditions was less effective. Analysis of electrical energy inputs showed that the hybrid NF/UV-sulfite process was competitive with other technologies for PFAS destruction. The UV treatment step and associated cooling requirements dominated energy inputs, which varied for different PFASs. Work aimed at optimizing passive cooling systems is recommended to further reduce energy requirements for PFAS remediation with this and related technologies.

## **Declaration of Competing Interest**

There are no conflicts of interest to declare.

# Acknowledgments

The funding for this project was supported by the United States Air Force Civil Engineering Center (AFCEC; BAA-031). The comments and views detailed herein may not necessarily reflect the views of AFCEC, its officers, directors, affiliates, or agents. The authors would like to thank Sharon Stone and Sean Houseworth (AFCEC) for their support in the field demonstration, Mike Veres and Tzahi Cath for their assistance in the field, Xylem, especially David Foster, for their support and coordination, Nathan Roth for his assistance in water quality analysis, and Anderson Ellis for his help in analysis.

#### Supplementary materials

Supplementary material associated with this article can be found, in the online version, at doi:10.1016/j.watres.2021.117677.

#### References

Appleman, T.D., Dickenson, E.R., Bellona, C., Higgins, C.P., 2013. Nanofiltration and granular activated carbon treatment of perfluoroalkyl acids. J. Hazard. Mater. 260, 740–746.

Bao, Y., Deng, S., Jiang, X., Qu, Y., He, Y., Liu, L., Chai, Q., Mumtaz, M., Huang, J., Cagnetta, G., Yu, G., 2018. Degradation of PFOA Substitute: GenX (HFPO–DA

C.J. Liu et al. Water Research 205 (2021) 117677

Ammonium Salt): oxidation with UV/persulfate or reduction with UV/sulfite? Environ. Sci. Technol. 52 (20), 11728–11734.

- Barzen-Hanson, K.A., Roberts, S.C., Choyke, S., Oetjen, K., McAlees, A., Riddell, N., McCrindle, R., Ferguson, P.L., Higgins, C.P., Field, J.A., 2017. Discovery of 40 classes of per- and polyfluoroalkyl substances in historical aqueous film-forming foams (AFFFs) and AFFF-impacted groundwater. Environ. Sci. Technol. 51 (4), 2047–2057.
- Bentel, M.J., Liu, Z., Yu, Y., Gao, J., Men, Y., Liu, J., 2020. Enhanced degradation of perfluorocarboxylic acids (PFCAs) by UV/Sulfite treatment: reaction mechanisms and system efficiencies at pH 12. Environ. Sci. Technol. Lett. 7 (5), 351–357.
- Bentel, M.J., Yu, Y., Xu, L., Li, Z., Wong, B.M., Men, Y., Liu, J., 2019. Defluorination of Per- and polyfluoroalkyl substances (PFASs) with hydrated electrons: structural dependence and implications to PFAS remediation and management. Environ. Sci. Technol. 53, 3718–3728.
- Buxton, G.V., Greenstock, C.L., Helman, W.P., Ross, A.B., 1988. Critical review of rate constants for reactions of hydrated electrons, hydrogen atoms and hydroxyl radicals (-OH/-O— in aqueous solution. J. Phys. Chem. Ref. Data 17 (2), 513–886.
- Cui, J., Gao, P., Deng, Y., 2020. Destruction of Per- and Polyfluoroalkyl Substances (PFAS) with advanced reduction processes (ARPs): a critical review. Environ. Sci. Technol. 54 (7), 3752–3766.
- Fujioka, T., Tu, K.L., Khan, S.J., McDonald, J.A., Roux, A., Poussade, Y., Drewes, J.E., Nghiem, L.D., 2014. Rejection of small solutes by reverse osmosis membranes for water reuse applications: a pilot-scale study 350, 28–34.
- Gu, Y., Liu, T., Wang, H., Han, H., Dong, W., 2017. Hydrated electron based decomposition of perfluorooctane sulfonate (PFOS) in the VUV/sulfite system. Sci. Total Environ. 607-608, 541–548.
- Guo, C., Zhang, C., Sun, Z., Zhao, X., Zhou, Q., Hoffmann, M.R., 2019. Synergistic impact of humic acid on the photo-reductive decomposition of perfluorooctanoic acid. Chem. Eng. J. 360, 1101–1110.
- Hu, X.C., Andrews, D.Q., Lindstrom, A.B., Bruton, T.A., Schaider, L.A., Grandjean, P., Lohmann, R., Carignan, C.C., Blum, A., Balan, S.A., Higgins, C.P., Sunderland, E.M., 2016. Detection of poly- and perfluoroalkyl substances (PFASs) in U.S. Drinking water linked to industrial sites, military fire training areas, and wastewater treatment plants. Environ. Sci. Technol. Lett. 3 (10), 344–350.
- Laura Del Moral, L., Choi, Y.J., Boyer, T.H, 2020. Comparative removal of Suwannee river natural organic matter and perfluoroalkyl acids by anion exchange: impact of polymer composition and mobile counterion. Water Res. 178, 115846.
- Le, T.X.H., Haflich, H., Shah, A.D., Chaplin, B.P., 2019. Energy-efficient electrochemical oxidation of perfluoroalkyl substances using a Ti<sub>4</sub>O<sub>7</sub> reactive electrochemical membrane anode. Environ. Sci. Technol. Lett. 6 (8), 504–510.
- Lee, S., Cho, J., Elimelech, M., 2005. Combined influence of natural organic matter (NOM) and colloidal particles on nanofiltration membrane fouling. J. Membr. Sci. 262 (1-2), 27-41.
- Liu, C.J., Strathmann, T.J., Bellona, C., 2021. Rejection of per- and polyfluoroalkyl substances (PFASs) in aqueous film-forming foam by high-pressure membranes. Water Res. 188, 116546.
- Liu, C.J., Werner, D., Bellona, C., 2019. Removal of per- and polyfluoroalkyl substances (PFASs) from contaminated groundwater using granular activated carbon: a pilotscale study with breakthrough modeling. Environ. Sci. Water Res. Technol. 5, 1844–1853.
- Moody, C.A., Field, J.A., 2000. Perfluorinated surfactants and the environmental implications of their use in fire-fighting foams. Environ. Sci. Technol. 34 (18), 3864–3870.
- Nau-Hix, C., Multari, N., Singh, R.K., Richardson, S., Kulkarni, P., Anderson, R.H., Holsen, T.M., Mededovic Thagard, S., 2021. Field demonstration of a pilot-scale

- plasma reactor for the rapid removal of poly- and perfluoroalkyl substances in groundwater. ACS EST Water 1 (3), 680–687.
- Nguyen, T.M.H., Bräunig, J., Thompson, K., Thompson, J., Kabiri, S., Navarro, D.A., Kookana, R.S., Grimison, C., Barnes, C.M., Higgins, C.P., McLaughlin, M.J., Mueller, J.F., 2020. Influences of chemical properties, soil properties, and solution pH on soil–water partitioning coefficients of per- and polyfluoroalkyl substances (PFASs). Environ. Sci. Technol. 54 (24), 15883–15892.
- Park, H., Vecitis, C.D., Cheng, J., Choi, W., Mader, B.T., Hoffmann, M.R., 2009.
  Reductive defluorination of aqueous perfluorinated alkyl surfactants: effects of ionic headgroup and chain length. J. Phys. Chem. A 113 (4), 690–696.
- Qanbarzadeh, M., Wang, D., Ateia, M., Sahu, S.P., Cates, E.L., 2020. Impacts of reactor configuration, degradation mechanisms, and water matrices on perfluorocarboxylic acid treatment efficiency by the UV/Bi3O(OH)(PO4)2 photocatalytic process. ACS ES&T Engineering 1 (2), 239–248.
- Qu, Y., Zhang, C.J., Chen, P., Zhou, Q., Zhang, W.X., 2014. Effect of initial solution pH on photo-induced reductive decomposition of perfluorooctanoic acid. Chemosphere 107, 218–223.
- Qu, Y., Zhang, C., Li, F., Chen, J., Zhou, Q., 2010. Photo-reductive defluorination of perfluorooctanoic acid in water. Water Res. 44 (9), 2939–2947.
- Rao, U., Su, Y., Khor, C.M., Jung, B., Ma, S., Cwiertny, D.M., Wong, B.M., Jassby, D, 2020. Structural dependence of reductive defluorination of linear PFAS compounds in a UV/electrochemical system. Environ. Sci. Technol. 54 (17), 10668–10677.
- Simon, J.A., Abrams, S., Bradburne, T., Bryant, D., Burns, M., Cassidy, D., Cherry, J., Chiang, S.Y., Cox, D., Crimi, M., Denly, E., DiGuiseppi, B., Fenstermacher, J., Fiorenza, S., Guarnaccia, J., Hagelin, N., Hall, L., Hesemann, J., Houtz, E., Koenigsberg, S.S., Lauzon, F., Longsworth, J., Maher, T., McGrath, A., Naidu, R., Newell, C.J., Parker, B.L., Singh, T., Tomiczek, P., Wice, R., 2019. PFAS experts symposium: statements on regulatory policy, chemistry and analytics, toxicology, transport/fate, and remediation for per- and polyfluoroalkyl substances (PFAS) contamination issues. Remediat. J. 29 (4), 31–48.
- Su, Y., Rao, U., Khor, C.M., Jensen, M.G., Teesch, L.M., Wong, B.M., Cwiertny, D.M., Jassby, D, 2019. Potential-driven electron transfer lowers the dissociation energy of the C–F bond and facilitates reductive defluorination of perfluorooctane sulfonate (PFOS). ACS Appl. Mater. Interfaces 11 (37), 33913–33922.
- Sun, Z., Zhang, C., Xing, L., Zhou, Q., Dong, W., Hoffmann, M.R., 2018. UV/ Nitrilotriacetic acid process as a novel strategy for efficient photoreductive degradation of perfluorooctanesulfonate. Environ. Sci. Technol. 52 (5), 2953–2962.
- Tenorio, R., Liu, J., Xiao, X., Maizel, A., Higgins, C.P., Schaefer, C.E., Strathmann, T.J., 2020. Destruction of per- and polyfluoroalkyl substances (PFASs) in aqueous filmforming foam (AFFF) with UV-sulfite photoreductive treatment. Environ. Sci. Technol. 54 (11), 6957–6967.
- USEPA Office of Water, 2016a. Drinking Water Health Advisory for Perfluorooctane Sulfonate (PFOS). EPA Document Number: 822-R-16-004.
- USEPA Office of Water, 2016. Drinking Water Health Advisory for Perfluorooctanoic Acid (PFOA). EPA Document Number: 822-R-16-005.
- Wu, B., Hao, S., Choi, Y., Higgins, C.P., Deeb, R., Strathmann, T.J., 2019. Rapid destruction and defluorination of perfluorooctanesulfonate by alkaline hydrothermal reaction. Environ. Sci. Technol. Lett. 6 (10), 630–636.
- Zarzo, D. and Prats, D. (2018) Desalination and energy consumption. What can we expect in the near future? Desalination 427, 1–9.
- Zepp, R.G., Braun, A.M., Hoigne, J., Leenheer, J.A., 1987. Photoproduction of hydrated electrons from natural organic solutes in aquatic environments. Environ. Sci. Technol. 21 (5), 485–490.